IN SILICO COMPUTATIONAL EXPLORATIONS OF SOME NOVEL PYRIMIDINE COMPOUNDS

Jyoti Maitry[1]*, Suman Uraiha[1], Lata Patel Choudhary[2] and Yogesh Pounikar[3]

[1]Post Graduate Student, Department of Pharmaceutical Chemistry, J. K. College of Pharmacy, Bilaspur 495550, Chhattisgarh, India.

[2]Associate Professor and Head, Department of Pharmacognosy, J. K. College of Pharmacy, Bilaspur 495550, Chhattisgarh, India.

[3]Professor, Department of Pharmacognosy, J. K. College of Pharmacy, Bilaspur 495550, Chhattisgarh, India.

*Corresponding Author

Jyoti Maitry

Post Graduate Student,

Department of

Pharmaceutical Chemistry,

J. K. College of Pharmacy,

Bilaspur 495550,

Chhattisgarh, India.

ABSTRACT

After searching several reputed pharmaceutical/medical databases such as PubMed, Scopus, etc., it was observed that not much information is available with Pyrimidine molecules due to limited substitutions, non-popularity, and difficulty in synthesis and therefore more vacuum and gaps have been identified in context to pharmacodynamics, pharmacokinetics, toxicity, metabolites, interactions, targeting, etc. The prime objectives of this research endeavors molecular docking studies against inflammatory target using Schrodinger software; *In silico* target identification studies using SWISS tool; and *In silico* pharmacokinetic profiling of Pyrimidine molecules using QuikProp module. The outcomes of this research point towards hands-on-experience of handling several online free computational chemistry tools and their interpretations, along with plausibility for the index study tag.

KEYWORDS: Pyrimidine, *In silico*, Pharmacokinetics, Toxicity, Computational, Docking.

INTRODUCTION

Pyrimidine is a six membered aromatic ring containing molecule with two nitrogens at 1 and 3 positions and belongs to the class of diazines (dia = two + azine = nitrogen). The ionization constant (pKa) of pyrimidine at monoprotonated state is 1.3, whereas pKa value of -6.9. It is

quite less basic than pyrimidine. It is a polar molecule with dipole moment ranges from 2.1 to 2.4 debye. Due to the presence of electronegetive nitrogen atom at 1 and 3 position the π-elcetron density at 2, 4 and 6 carbon atom of the ring is less and are π-electron deficient.[1] Due to inductive elcetronegetive effect position 5 of pyrimidine ring is also electron deficient but less than 2,4 and 6 positions. Pyrimidine has a relatively low melting point of around 20-22°C and a boiling point of approximately 123-124°C. These values may vary depending on the specific substitution pattern on the pyrimidine ring. Pyrimidine is sparingly soluble in water but more soluble in organic solvents such as ethanol, methanol, and acetone. The solubility in water can be enhanced by the addition of polar functional groups or by adjusting the pH of the solution.[2] Pyrimidine is weakly basic due to the lone pair of electrons on its nitrogen atoms. It can act as a Lewis base by donating these electrons to form coordination complexes with Lewis acids. However, pyrimidine is also capable of accepting protons, albeit less readily than its derivative, pyrimidine. Pyrimidine is a basic building block of nucleotides, which are the structural units of nucleic acids like DNA and RNA. In DNA, pyrimidines specifically refer to the nucleobases cytosine (C) and thymine (T), while in RNA, uracil (U) replaces thymine. These nucleobases pair with purines (adenine and guanine) to form the complementary base pairs that stabilize the double helical structure of DNA and RNA molecules.[3]
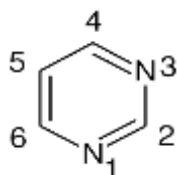

Pyrimidine scaffold is a highly privileged pharmacophore in medicinal chemistry as it exhibited excellent pharmacological activities like antimicrobial, analgesic, anticancer, anti-inflammatory, antioxidant, analgesic, antiviral, antidiabetic, antirheumatic, antihypertensive, antileishmanial, anti-alzheimer and antimalarial.[4] Indispensible importance and role of pyrimidine nucleus in medical science could be understood from the fact that it served as a basic pharmacophore in most of the clinically used drugs. Various scientists and researchers still working on designing and development of more potent, selective, and safer pyrimidine-based molecules for the treatment of various diseases. Pyrimidine has long been recognized as a crucial building block in drug discovery and development. Its unique chemical properties make it a versatile and indispensable component in the synthesis of pharmaceuticals. It explores the pivotal role of pyrimidine in drug discovery processes.[5]

After searching several reputed pharmaceutical/medical databases such as PubMed, Scopus, etc., it was observed that not much information is available with Pyrimidine molecules due to limited substitutions, non-popularity, and difficulty in synthesis and therefore more vacuum and gaps have been identified in context to pharmacodynamics, pharmacokinetics, toxicity, metabolites, interactions, targeting, etc. These gaps encouraged us to study the physical, chemical, biological, pharmacological, etc. perspectives of Pyrimidine molecules using available free tools.

MATERIALS AND METHODS

Dataset
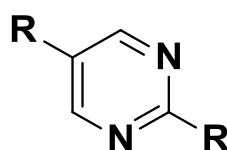
S. No.	R	S. No.	R	S. No.	R
1.	CH_3	2.	CF_3	3.	SO_3H
4.	OH	5.	Cl	6.	SO_2NH_2
7.	NH_2	8.	Br	9.	COCl
10.	NO_2	11.	F	12.	CN
13.	OCH_3	14.	I	15.	COOH

Molecular Docking

Preparation of Ligand

The 3D structures of chosen ligands, Pyrimidine was obtained in ".sdf" format using PubChem (https://pubchem.ncbi.nlm.nih.gov/). PubChem is an open-access database of chemical substances and biological activity. The method addressed the docking issue using flexible ligands and moveable protein atoms. The Avogadro programme was used to add hydrogen atoms to ligands, and the MMFF94 force field is utilized to compute the energy of the protein-ligand combination for every given configuration without any fitting parameters.[6]

Preparation of Protein

3D crystalline target structures were downloaded from the Protein Data Bank (PDB). The target was created by removing all water molecules beyond 5A°, assigning disulfide links, bond order, and formal charges, and removing metal ions, co-factors, and heterogroup from the useable preprocessed and studied structure. With the assistance of the H-bond assignment technique, the hydrogen atoms as well as the hydrogen-bonding network was optimized.

Molecular docking was used to estimate receptor grids for protein targets where the ligand would mix within the predicted active site. The grids (cubic boxes with defined dimensions) encompass the whole ligand and were built at the ligand's centroid (crystallized with the target structure). The grid box size was increased to 126 A°, 126 A° and 126 A° (x, y, and z, respectively) to include all of the amino acid residues present in stiff macromolecules. The Auto Grid 4.2, which came with Auto Dock 4.2, was used to generate grid maps. The grid points was 0.375° apart. The Van der Waals scale factor was set to 1.0, while the charge cutoff was set at 0.25. Induced-fit docking (IFD) was conducted on each ligand, and the lowest resulting score for the best-docked posture was confirmed.[7]

Induced-Fit Molecular Docking (IFD)

The IFD was created utilizing the structure-based drug design technique, which involves rendering precise geometry ligands to dock with a biological target's defined structure. The free-state ligands are docked into the rigid state receptor's active site, enzyme, tube, etc., resulting in a predicted binding mode and the strength of the fit being evaluated. In receptor-based computational techniques, the attachment of a low-molecular-weight ligand to a macromolecular protein has its own significance since the most suitable connection with low energy values and possible steric conflicts is found. To investigate a particular docking issue, Auto Dock provides a number of search methods. In this study, the Lamarckian Genetic Algorithm (LGA) was employed to identify the best conformers. During the docking process, a maximum of 10 conformers was evaluated. The population was limited to 150 individuals, who was selected at random. The mutation rate was set to 0.02 and the crossover rate was set to 0.8. The maximum number of energy evaluations was set to 500000, the maximum number of generations was set to 1000, the maximum number of top individuals that automatically survived was set to 1. Translations had a 0.2 step size, quaternions had a 5.0° step size, and torsions had a 5.0° step size. Cluster tolerance was set to 0.5, external grid energy to 1000.0, maximum binding energy to 0.0, maximum number of retries to 10000, and 10 LGA runs was performed. The interactions and binding energy of the docked structure was studied using the Auto Dock findings. It was performed many times to get different docked conformations as well as to assess anticipated docking energy. The optimal ligand-receptor structure was selected among the docked structures based on the ligand's lowest energy and minimum solvent accessibility. The Accelrys Visualizer discovery studio tool was used to visualize the docking findings.[8]

Pharmacokinetics, Bioavailability, and Drug-likeliness studies

The SwissADME online tool was used to conduct a prediction research of pharmacokinetics, namely ADME, bioavailability, and drug-likeness of ligands. To identify drug-likeness, the technology estimates bioavailability radar based on six physicochemical properties: lipophilicity, size, polarity, insolubility, flexibility, and insaturation. The ADME properties, such as passive human gastrointestinal absorption (HIA) and blood-brain barrier (BBB) permeation, as well as substrate or non-substrate of the permeability glycoprotein (P-gp) was detected positive or negative in the BOILED-Egg model within the tool. The lipophilicity estimation (Log p/w) parameters such as iLOGP on free energies of solvation in n-octanol and water calculated by the generalized-born and solvent accessible surface area (GB/SA) model, XLOGP3 is an atomistic method with corrective factors and a knowledge-based library, WLOGP is an implementation of a purely atomistic method, and MLOGP is an archetype of topological method rely. The Lipinski (Pfizer) filter, which was the first rule-of-five to be implemented in a tool, was used to predict drug-likeness. The bioavailability radar was used to predict oral bioavailability based on several physicochemical characteristics.[9]

Drug Target Identifications

SwissTargetPrediction is a web service for bioactive small molecule target prediction. This website enables to anticipate a tiny molecule's targets. It compares the query molecule to a library of 280,000 molecules active on more than 2000 targets in five distinct species using a mix of 2D and 3D similarity metrics. Understanding the molecular processes behind bioactivity and anticipating possible side effects or cross-reactivity requires mapping the targets of bioactive small compounds. Predictions have been made in three distinct organisms (models), and for near paralogs and orthologs, mapping predictions by homology within and across species is possible. The human (*Homo sapiens*), rat (*Rattus norvegicus*), and mouse (*Mus musculus*) models have all been shown to have credible inhibitory targets for the molecules.[10]

Molecular simulation study

The molecular dynamics simulation of the ligand was done using the GROMACS simulation Package and CHARMM 27 force field. To obtain the molecular topology file compatible with the CHARMM 27 force field, SwissParam web service was utilized to explicit water model, the protein-ligand assembly was solvated and the completely system was neutralized with the addition of Na ions by replacing the water molecules. After completing these steps, the

energy minimization of the system was done, which was followed by equilibration of the system using two consecutive NVT (5 ns) and NPT (5 ns) runs. To fix all NVT and NPT runs, the V-rescale thermostat and Berendsen barostat for temperature (298 K) and pressure (1 bar) were used, respectively. Finally, the resulting ensembles were introduced to 40ns MD simulation with a time-stage of 2 fs for each simulation. Cut-off ratios of 1 nm and smooth Particle Mesh Ewald (PME) protocol was used for treat the long-range electrostatic interactions The snapshots of simulation trajectories was observed using visual molecular dynamics (VMD) software. Root mean square deviation (RMSD) of peptide (atom backbone), radius of gyration (Rg) and root-mean-square fluctuation (RMSF) values was plotted using XMGRACE.[11]

Degradation pathways for molecules

Start by installing Spartan on a compatible workstation and ensure that the software is properly licensed and activated. Once installed, open Spartan and configure the initial settings, such as selecting the appropriate computational resources (e.g., number of CPU cores) and defining the working directory where all project files will be stored. Begin by constructing the molecular structure of the compound of interest. In Spartan, this can be done using the Build tool. Use the provided atom and bond tools to create the molecule, ensuring that the structure is accurate. Spartan also allows you to import structures from external databases or files (e.g., .mol, .pdb, or .xyz formats). After constructing the molecule, perform a preliminary geometry optimization to correct any structural issues and to ensure that the molecule is in a reasonable starting conformation. With the molecule constructed, proceed to the Setup menu and select the Calculations option. Choose Geometry Optimization from the list of available calculations. Select an appropriate level of theory, such as Density Functional Theory (DFT) with a specific functional (e.g., B3LYP) and basis set (e.g., 6-31G*). Depending on the size and complexity of the molecule, you may choose higher levels of theory for more accurate results. Start the geometry optimization calculation and monitor the progress. Spartan will iterate through different conformations to find the lowest energy structure, which represents the most stable form of the molecule. Once the geometry optimization is complete, perform a frequency analysis to ensure that the optimized structure is at a true minimum on the potential energy surface. This step is crucial for confirming the stability of the structure and identifying any potential reactive sites or bond strains that could influence degradation pathways. Access this feature again through the Setup menu by

selecting Vibrational Frequencies from the calculation types. After the calculation is finished, analyze the results to check for any imaginary frequencies.[12]

RESULTS AND DISCUSSION

Molecular Docking

The structure of novel Pyrimidine derivatives were sent for induced fit docking study by using Glide software and this docking result confirms that our compound has anti-inflammatory activity. The molecular docking scores of 15 novel pyrimidine compounds, ranging from -5.75 Kcal/mol to -8.62 Kcal/mol, provide valuable insights into their potential binding affinities with the target protein. These scores reflect the predicted free energy of binding between the ligand (pyrimidine compound) and the receptor (target protein), serve as an indicator of how strongly each compound is likely to interact with the protein. Generally, lower (more negative) docking scores indicate stronger binding affinities, suggesting that the compound may form a more stable and potent interaction with the target.

Among the compounds, Compound-9, with a docking score of -8.62 kcal/mol, shows the strongest binding affinity, indicating that it is likely to form the most stable interaction with the target protein. This makes Compound-9 a particularly promising candidate for further investigation, as it may have a higher potential for therapeutic efficacy. Following closely, Compound-6 (-8.34 kcal/mol) and Compound-2 (-8.19 kcal/mol) also exhibit strong binding affinities, suggesting that these compounds could similarly be effective in interacting with the target protein. These three compounds stand out as the most promising among the set due to their superior docking scores.

Compound-3 (-7.73 kcal/mol), Compound-4 (-7.67 kcal/mol), Compound-5 (-7.28 kcal/mol), and Compound-7 (-7.16 kcal/mol) fall into the intermediate range, with moderately strong binding affinities. These compounds may still have potential as effective therapeutic agents, though they may require further optimization to enhance their binding efficiency. Their docking scores suggest that they form relatively stable interactions with the target, but they might not be as potent as the top three compounds.

On the lower end of the spectrum, Compound-10 (-5.75 kcal/mol), Compound-11 (-5.99 kcal/mol), and Compound-15 (-6.13 kcal/mol) show the weakest binding affinities among the group. While these scores suggest that the interactions between these compounds and the target protein may be less stable, these compounds are not without potential. They could

serve as starting points for structure-based optimization to improve their binding affinities or might be more effective against alternative targets. Compound-1 (-6.51 kcal/mol), Compound-8 (-6.53 kcal/mol), Compound-12 (-6.93 kcal/mol), Compound-13 (-6.49 kcal/mol), and Compound-14 (-6.58 kcal/mol) occupy a middle ground in terms of binding affinity. These compounds show moderate interaction potential, suggesting that they might be effective under certain conditions or with further modifications to enhance their binding properties.

The molecular docking data indicates that Compound-9, Compound-6, and Compound-2 (**Table 1**) are the most promising candidates due to their strong binding affinities. These compounds should be prioritized for further *in vitro* and *in vivo* studies to validate their therapeutic potential. The other compounds, while showing varying degrees of binding affinity, also present opportunities for further exploration and optimization. This range of docking scores highlights the diverse potential of the pyrimidine compounds and sets a foundation for the next steps in drug development. Compound-9 has been selected as ideal compound due to highest docking interaction score amongst the 15 pyrimdine compounds series and further investigations were done against multiple inflammatory targets (COX-2, 5LOX, and TXA-2).

Table 1: Glide scores of novel Pyrimidine derivatives against COX-1.

Compound	Energy (Kcal/mol)
1	-6.51
2	-8.19
3	-7.73
4	-7.67
5	-7.28
6	-8.34
7	-7.16
8	-6.53
9	-8.62
10	-5.75
11	-5.99
12	-6.93
13	-6.49
14	-6.58
15	-6.13

The induced fit molecular docking studies confirmed the interaction of the Compound-9 scaffold with the inflammatory mediator COX-1, COX-2, LOX-5, and TXA-2. The result of

Compound-9 for COX-1 inhibitory potential and PLA-2 inhibitory potential are more promising. The Compound-9 displayed a notable glide score for COX-1, COX-2, and PLA-2. The Compound-9 displayed notable Glide scores of -8.62 Kcal/mol for COX-1 and exhibited interaction through hydrogen bonding with GLYB45 residue. For COX-2, the Compound-9 displayed notable Glide scores of -6.61 Kcal/mol and exhibited interaction through pie-alkyl bonding with LYSD454 and ARGD29 residues. The Compound-9 displayed notable Glide scores of -6.15 Kcal/mol for LOX-5 and exhibited interaction through pie-alkyl bonding with LYSA196, TRPA198, and LEUA154 as well hydrogen bonding with TRPA198 residue. The Compound-9 displayed notable Glide scores of –5.34 Kcal/mol for TXA-2 and exhibited interaction through pie-alkyl bonding with VALA111, LEUA161, and VALA110, TRPA157, and LEUA76 as well pi-pi bonding with PHEA107 residue and pi-sulfur bonding with PHEA114 residue (**Table 2**).

Table 2: Glide scores of Compound-9 as inflammatory enzymes inhibitor.

S. No.	Target	Energy (Kcal/mol)
1.	COX-1	-8.62
2.	COX-2	-6.61
3.	LOX-5	-6.15
4.	TXA-2	-5.34

COX-1 inhibitory potential

The induced fit molecular docking studies confirmed the interaction of the synthesized Schiff base scaffold with the inflammatory mediator COX-1. The Schiff base displayed notable Glide scores of -8.62 Kcal/mol and exhibited interaction through hydrogen bonding with GLY B45 residue and pi-alkyl bonding with PRO B130, LEU B152, CYS B47, VAL B48, and ILE B46 (**Figure 1**).
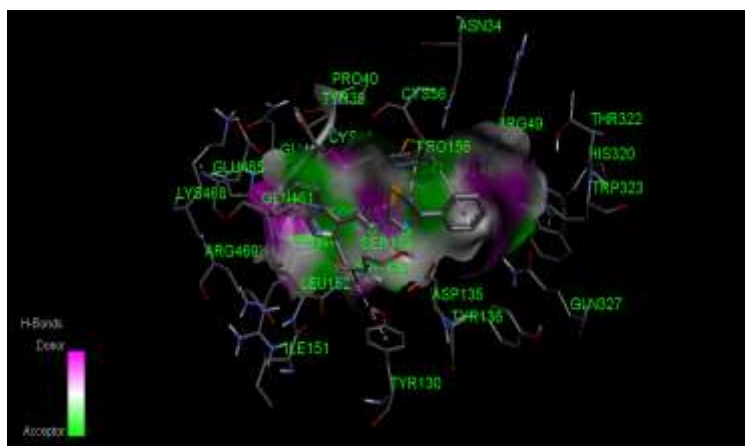

Figure 1: 3D binding modes and interactions of the Compound-9 with COX-1 enzyme.

COX-2 inhibitory potential

The induced fit molecular docking studies confirmed the interaction of the synthesized Schiff base scaffold with the inflammatory mediator COX-2. The Schiff base displayed notable Glide scores of-6.61 Kcal/mol and it exhibited interaction through alkyl bonding with ARG D:29 and LYS D:454 (**Figure 2**).
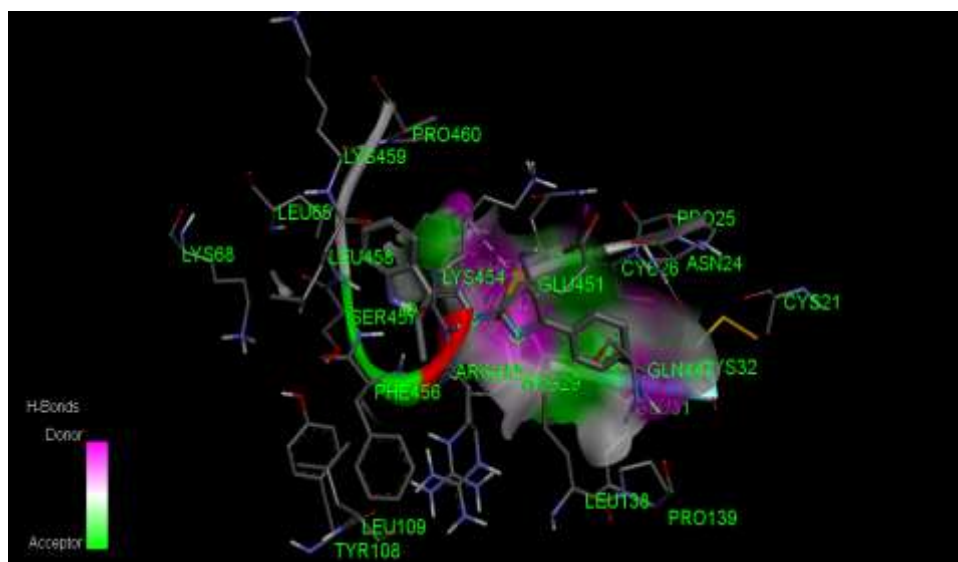

Figure 2: 3D binding modes and interactions of Compound-9 with COX-2 enzyme.

LOX-5 inhibitory potential

The Schiff base displayed notable Glide scores of -6.15 Kcal/mol and exhibited interaction through pie-alkyl bonding with LYS A196, TRP A198, and LEU A154 as well hydrogen bonding with TRP A198 residue (**Figure 3**).
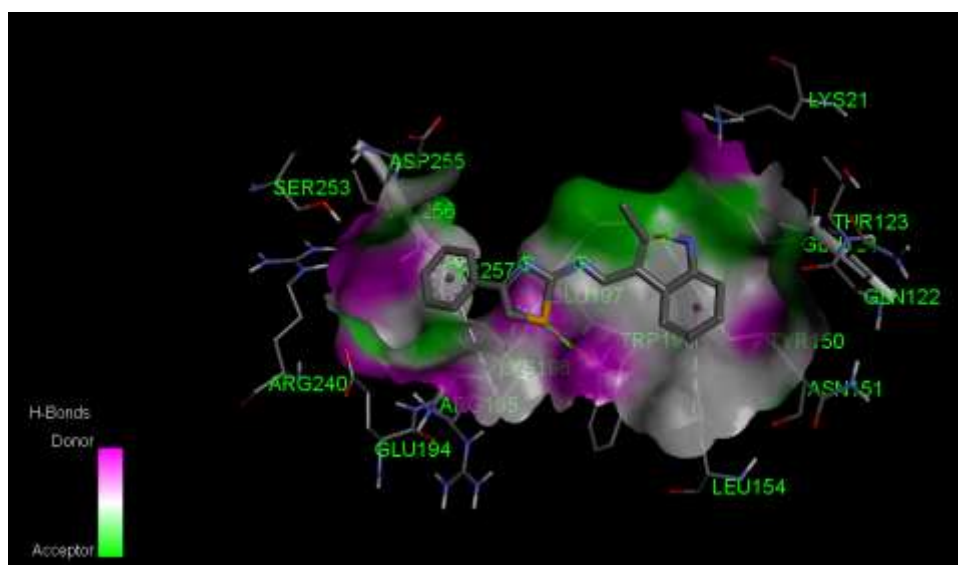

Figure 3: 3D binding modes and interactions of Compound-9 with LOX-5 enzyme.

TXA-2 inhibitory potential

The Schiff base displayed notable Glide scores of −5.34 Kcal/mol and exhibited interaction through pie-alkyl bonding with VAL A111, LEU A161, VAL A110, TRP A157, and LEU A76 as well pi-pi bonding with PHE A107 residue and pi-sulfur bonding with PHE A114 residue (**Figure 4**).
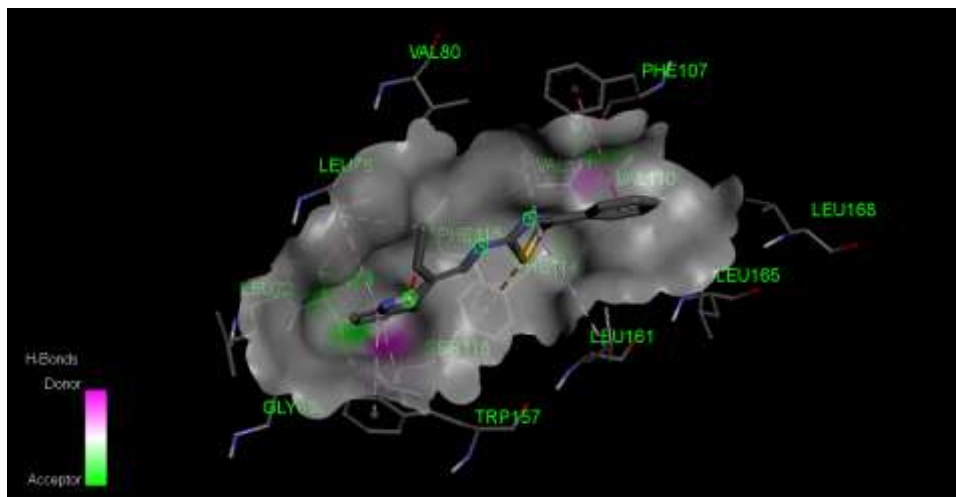

Figure 4: 3D binding modes and interactions of Compound-9 with TXA-2 enzyme.

The study provided directions towards the rational development of anti-inflammatory agents by deciphering the essential structural requirements and substituents for modulation. The position and the number of hydrogen group were found to be a necessary aspect of designing better inhibitors.

Molecular Simulations

When proteins undergo major conformational changes during interactions with medicinal compounds, molecular dynamics simulations (MDS) serve an important role in understanding the internal motion, conformational variations, stability, and so on of protein-ligand complexes. The dynamic behavior of Pyrimidine derivative (Compound-9) within COX-1 was investigated using a 100 ns MD simulation study of all atoms. A number of parameters, including the protein Cα atoms Root Mean Square Deviation (RMSD), ligand RMSD with respect to protein, Root Mean Square fluctuation (RMSF), and protein-ligand contact analysis, were estimated from the complete MD-simulated trajectories to analyze the dynamic nature and stability of the ligand-bound with the main protease protein. The divergence of the protein Cα atoms associated with drug molecules can be explained by the RMSD value from the MD trajectory. **Figure 5A** depicts the RMSD plots against simulation time, where modest

fluctuations imply the achievement of a stable conformation and *vice versa*. It revealed that the complex RMSD initially fluctuated between 2.1Å and 2.7Å over the first 18 ns, followed by steady stability and a mean value of 2.2Å for the remainder of the simulation. Due to equilibration, the ligand RMSDs fluctuated with a maximum value of 4.2Å within the first 10 ns, followed by more stable interactions for the duration of the simulation.

To assess the mobility of the complex, the RMSF graph of each amino acid residue as a function of residue number is displayed in **Figure 5B**. A high RMSF value implies protein structural flexibility, loose bonding, or the existence of loops; a low value shows stability and the occurrence of secondary structures such as sheets and helices. The peak in this plot represents the residues that fluctuate the most throughout the simulation. The variations began at 0.5Å and progressed to 2.5Å, with the majority of the fluctuations occurring in the -C and -N terminals. In this complex, Pyrimidine derivative (Compound-9) interacted with 21 amino acids of COX-1 protein including Thr24 (1.05Å), Thr25 (0.757Å), Cys44 (0.768Å), Thr45 (1.272Å), Ser46 (1.262Å), Met49 (0.932Å), Asn142 (0.928Å), Cys145 (0.492Å), Tyr154 (1.172Å), Met165 (0.602Å), Glu166 (0.644Å), Leu167 (0.714Å), Pro168 (1.146Å), Arg188, (0.834Å), Gln189 (1.143Å), Thr190 (1.156Å), Ala191 (1.514Å), Gln192 (1.097Å), Pro252 (1.067Å), Ala255 (1.141Å), and Gln256 (1.171Å). The obtained low values probably explained no amino acid residues fluctuated significantly during the simulation. In Pyrimidine derivative (Compound-9), polar terminal hydroxyl interacted with Gln192 and Thr190 through amino acid-mediated hydrogen bonding and direct hydrogen bonding, respectively. Similarly, Gln189 and Ser46 show hydrogen bonding with the carbonyl oxygen of the terminal ester group at 15% and 16% of simulation time, respectively.

For the stability of a ligand-protein complex, the presence of a large number of intermolecular interactions is very crucial. As seen in the graphic above, these interactions may be classified and summarized by type. Protein-ligand interactions are classified into four types: hydrogen bonds, hydrophobic interactions, ionic interactions, and water bridges. The stacked bar charts are normalized throughout the trajectory: for example, a value of 0.5 indicates that the specific contact is maintained 50% of the time during the simulation. Values greater than 1.0 are achievable because a protein residue may have several interactions with the same subtype of ligand. In this complex, Met165 shows the major interaction though hydrophobically, which is 70% of the simulation time (**Figure 5C**). The RMSD, RMSF, and protein-ligand contact analysis parameters derived from the MD simulation trajectory

demonstrated that the protein-ligand complex stayed stable in dynamic states, and the proposed COX-1 protein inhibitor was maintained inside the receptor cavity.
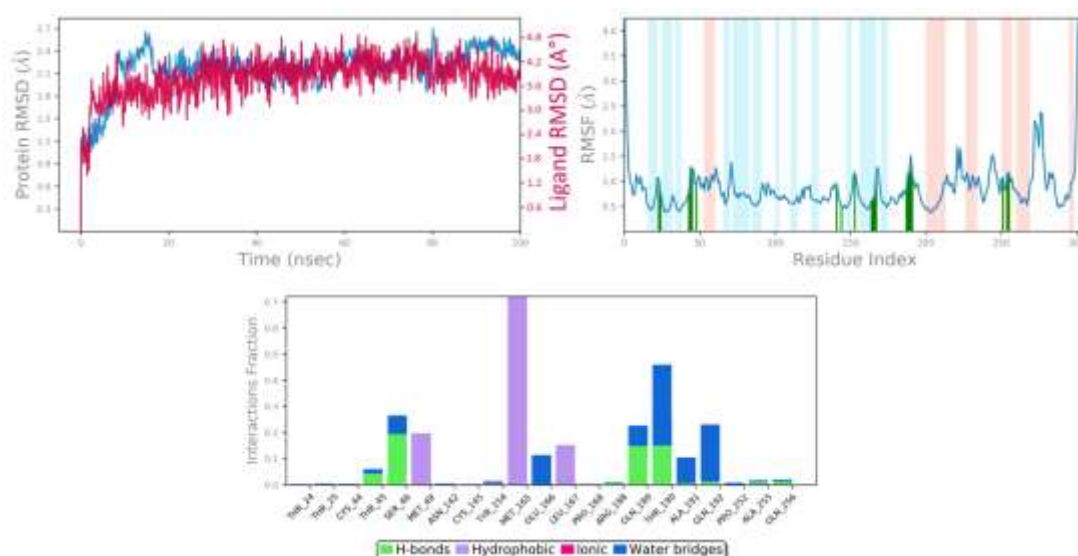

Figure 5: MD simulation analysis of Pyrimidine derivative (Compound-9) in complex with COX-1 (A) RMSD (Protein RMSD is shown in grey while RMSD of compound Pyrimidine derivative (Compound-9) are shown in red) (B) Protein RMSF, and (C) Protein–ligand contact analysis of MD trajectory.
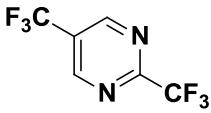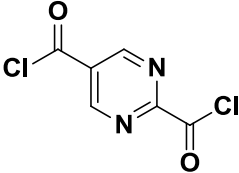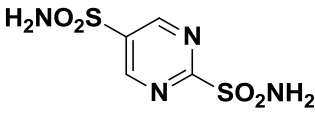
Pharmacokinetics, Bioavailability, and Drug-likeliness studies

Table 3 describes the predictive values for pharmacokinetics, bioavailability and drug-likeness data on novel Pyrimidine derivative. Compound-2 showed high absorption rate. Good blood-brain permeability was obtained based on LogP value while low negative value indicated less skin permeation. In case of metabolism, the molecule did not prove to be a p-glycoprotein substrate. It acts as CYP_{450} inhibitors and specifically inhibits CYP1A2 and CYP2D6 isoforms. For the prediction of bioavailability and drug-likeness, a moderate bioavailability score was obtained. Poor water soluble characteristics were obtained for the novel Pyrimidine derivative.

Compound-6 showed high absorption rate. Good blood-brain permeability was obtained based on LogP value while moderate negative value indicated less skin permeation. In case of metabolism, the molecule did prove to be a p-glycoprotein substrate. It acts as CYP_{450} inhibitors and specifically inhibits CYP2D6 isoform. For the prediction of bioavailability and drug-likeness, a moderate bioavailability score (0.55) was obtained. Poor to moderate water soluble characteristics were obtained for this novel Pyrimidine derivative.

Compound-9 showed low absorption rate. Poor blood-brain permeability was obtained based on LogP value while low negative value indicated less skin permeation. In case of metabolism, the molecule did prove to be a p-glycoprotein substrate. It acts as CYP_{450} inhibitors and specifically inhibits CYP2C19 and CYP2D6 isoforms. For the prediction of bioavailability and drug-likeness, a moderate bioavailability score (0.55) was obtained. Poor water soluble characteristics were obtained for the novel Pyrimidine derivative.

Table 3: Pharmacokinetics and physicochemical properties of novel Pyrimidine derivatives.

Properties	Compound-2	Compound-6	Compound-9
Physicochemical Properties			
Structure			
Formula	$C_6H_2F_6N_2$	$C_6H_2Cl_2N_2O_2$	$C_4H_6N_4O_4S_2$
Molecular weight (g/mol)	216.01	203.95	237.98
Number of heavy atoms	26	27	26
Number of aromatic heavy atoms	12	12	12
Fraction Csp^3	0.48	0.50	0.50
Number of rotatable bonds	7	8	7
Number of H-bond acceptors	2	2	1
Number of H-bond donors	2	1	1
Molar Refractivity	111.71	116.18	114.65
TPSA (A^2)	35.05	24.50	15.27
SMILES	O=C(CCCCC1=CC=CC=C1)/C=C/C2=CC=C(OS(C3=CC=C(Cl)C=C3)(=O)=O)C(OC)=C2	O=C(CCCCC1=CC=CC=C1)/C=C/C2=CC=C(OS(Cl)=O)C(OC)=C2	O=C(CCCCC1=CC=CC=C1)/C=C/C2=CC=C(OS©(=O)=O)C(OC)=C2
Lipophilicity			
Log Po/w (Ilogp)	3.67	4.42	4.40
Log Po/w (XLOGP3)	5.99	6.32	6.71
Log Po/w (WLOGP)	5.53	5.84	6.14

Log Po/w (MLOGP)	4.05	4.26	4.87
Log Po/w (SILICOS-IT)	4.65	5.20	5.66
Consensus Log Po/w	4.78	5.21	5.56
Water Solubility			
Log S (ESOL)	-5.68	-5.90	-6.12
Solubility	7.39e-04 mg/ml ; 2.09e-06 mol/l	4.67e-04 mg/ml ; 1.27e-06 mol/l	2.66e-04 mg/ml ; 7.58e-07 mol/l
Class	Moderate Soluble	Moderate Soluble	Poorly Soluble
Log S (Ali)	-6.51	-6.62	-6.83
Solubility	1.08e-04 mg/ml ; 3.07e-07 mol/l	8.71e-05 mg/ml ; 2.38e-07 mol/l	5.13e-05 mg/ml ; 1.46e-07 mol/l
Class	Poorly Soluble	Poorly Soluble	Poorly Soluble
Log S (SILICOS-IT)	-6.83	-7.53	-7.80
Solubility	5.17e-05 mg/ml ; 1.47e-07 mol/l	1.09e-05 mg/ml ; 2.97e-08 mol/l	5.58e-06 mg/ml ; 1.59e-08 mol/l
Class	Poorly Soluble	Poorly Soluble	Poorly Soluble
Pharmacokinetics			
GI absorption	High (93.747%)	High (94.736%)	Low (83.636%)
BBB permeant	Yes (-0.942)	Yes (-0.168)	No
CNS permeability	-2.159	-2.337	-2.281
P-gp substrate	No	Yes	Yes
Caco2 permeability	0.421	1.131	0.943
CYP1A2 inhibitor	Yes	No	No
CYP2C19 inhibitor	No	No	Yes
CYP2C9 inhibitor	No	No	No
CYP2D6 inhibitor	Yes	Yes	Yes
CYP3A4 inhibitor	No	No	No
Log Kp (skin permeation) (cm/s)	-4.20	-4.05	-3.67
Total clearance (log ml/min/kg)	-0.317	-0.106	-0.462
Renal OCT2 substrate	No	No	No
Toxicity			
Minnow toxicity	-1.583	-1.013	-1.083

(log mM)			
T. pyriformis toxicity (log ug/L)	0.295	1.099	1.259
Oral Rat Acute Toxicity (LD_{50}) (mol/kg)	2.349	2.577	2.667
Oral Rat Chronic Toxicity (LOAEL) (log mg/kg_bw/day)	1.17	1.287	1.374
Max. tolerated dose (human) (log mg/kg/day)	0.321	0.787	0.344
Hepatotoxicity	No	No	No
Skin Sensitisation	No	No	No
AMES toxicity	No	No	No
Drug-likeness			
Lipinski	Yes; 0 violation	Yes; 1 violation: MLOGP>4.15	Yes; 1 violation: MLOGP>4.15
Ghose	Yes	No; 1 violation: WLOGP>5.6	No; 1 violation: WLOGP>5.6
Veber	Yes	Yes	Yes
Egan	Yes	Yes	No; 1 violation: WLOGP>5.88
Muegge	No; 1 violation: XLOGP3>5	No; 1 violation: XLOGP3>5	No; 1 violation: XLOGP3>5
Bioavailability Score	0.55	0.55	0.55
Medicinal Chemistry			
PAINS	0 alert	0 alert	0 alert
Brenk	1 alert: hydroquinone	0 alert	0 alert
Lead-likeness	No; 2 violations: MW>350, XLOGP3>3.5	No; 3 violations: MW>350, Rotors>7, XLOGP3>3.5	No; 2 violations: MW>350, XLOGP3>3.5
Synthetic accessibility	3.19	3.30	3.28

Bioavailability Radar Plot

The bioavailability radar of Compound-2 for oral bioavailability prediction showed desired INSATU = insaturation as per Csp^3 as 0.48, FLEX as per number of rotable bond 7, INSOLU Logs (ESOL) as -5.68 (insoluble), SIZE as molecular weight (g/mol) of 329.04, POLAR as TPSA (Å²) 35.05, and LIPO as XLOGP3 value of 5.99 (**Figure 6A**). The bioavailability radar of Compound-6 for oral bioavailability prediction showed desired INSATU = insaturation as

per Csp[3] as 0.50, FLEX as per number of rotable bond 8, INSOLU Logs (ESOL) as -5.90 (insoluble), SIZE as molecular weight (g/mol) of 366.54, POLAR as TPSA (Å²) 24.50, and LIPO as XLOGP3 value of 6.32 (**Figure 6B**). The bioavailability radar of Compound-9 for oral bioavailability prediction showed desired INSATU = insaturation as per Csp[3] as 0.50, FLEX as per number of rotable bond 7, INSOLU Logs (ESOL) as -6.12 (insoluble), SIZE as molecular weight (g/mol) of 350.54, POLAR as TPSA (Å²) 15.27, and LIPO as XLOGP3 value of 6.71 (**Figure 6C**).
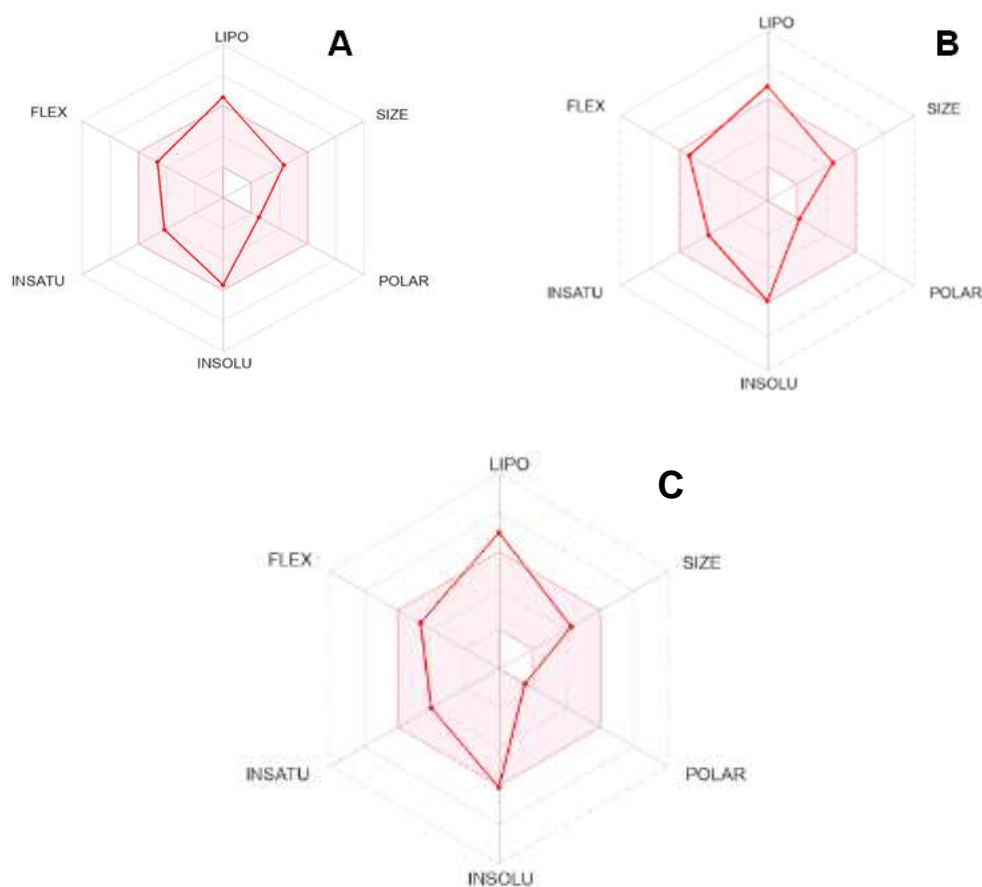

Figure 6: Bioavailability Radar Plot (A) Compound-2, (B) Compound-6, and (C) Compound-9.

Boiled Egg Plot

In case of BOILED-Egg model (**Figure 7**), the Brain Or Intestina LEstimateD permeation method (BOILED-Egg) has already been proposed as an accurate predictive model, which helps by computational prediction of the lipophilicity and polarity of small molecules. In overall predictive results, novel Pyrimidine derivative can be suitable drug candidate as per bioavailability radar and BOILED-Egg representation. It was observed in the predictions that

Compound-2 (**Figure 7A**) was a PGP positive non-substrate. PGP positive non-substrate molecules are compounds that interact with P-glycoprotein but are not themselves transported by it. These molecules can influence PGP activity in several ways, such as inhibiting or activating its transport function, altering its expression levels, or modulating its conformation. Unlike substrates that are actively pumped out of cells by PGP, non-substrate molecules bind to PGP and affect its function without being expelled. It was obtained that novel Pyrimidine derivative, Compound-6 (**Figure 7B**) has limited capability of blood-brain barrier penetration as well as it also showed low gastrointestinal absorption. The molecule was found to be PGP positive as non-substrate in predictive model. PGP positive non-substrate behaviour was observed in the predictions for Compound-9 (**Figure 7C**). PGP positive non-substrate molecules represent a significant area of interest in pharmacology and drug development. By modulating the function and expression of P-glycoprotein, these molecules offer potential strategies for overcoming multidrug resistance, optimizing drug pharmacokinetics, and enhancing therapeutic efficacy. Ongoing research continues to explore and develop new PGP inhibitors and modulators, aiming to address the challenges posed by drug resistance and improve patient outcomes across various medical conditions.
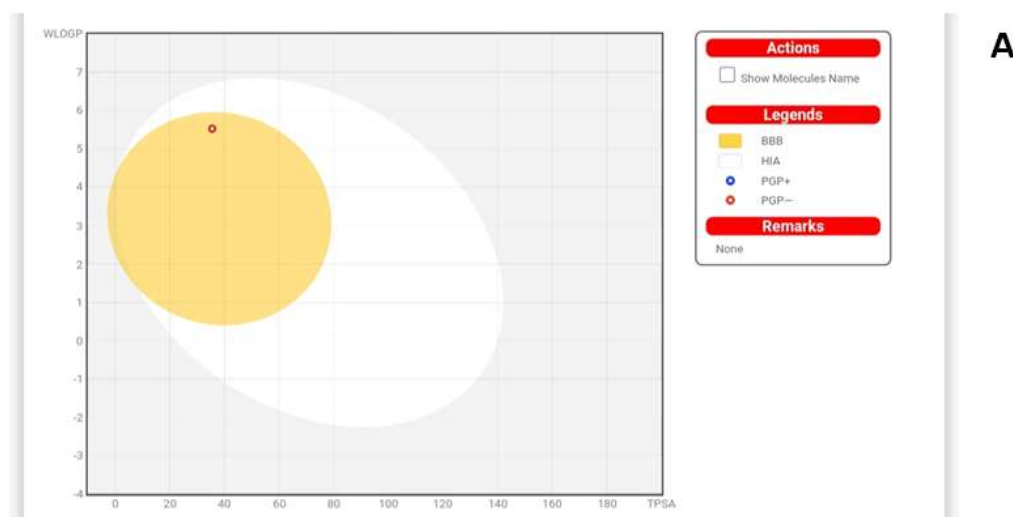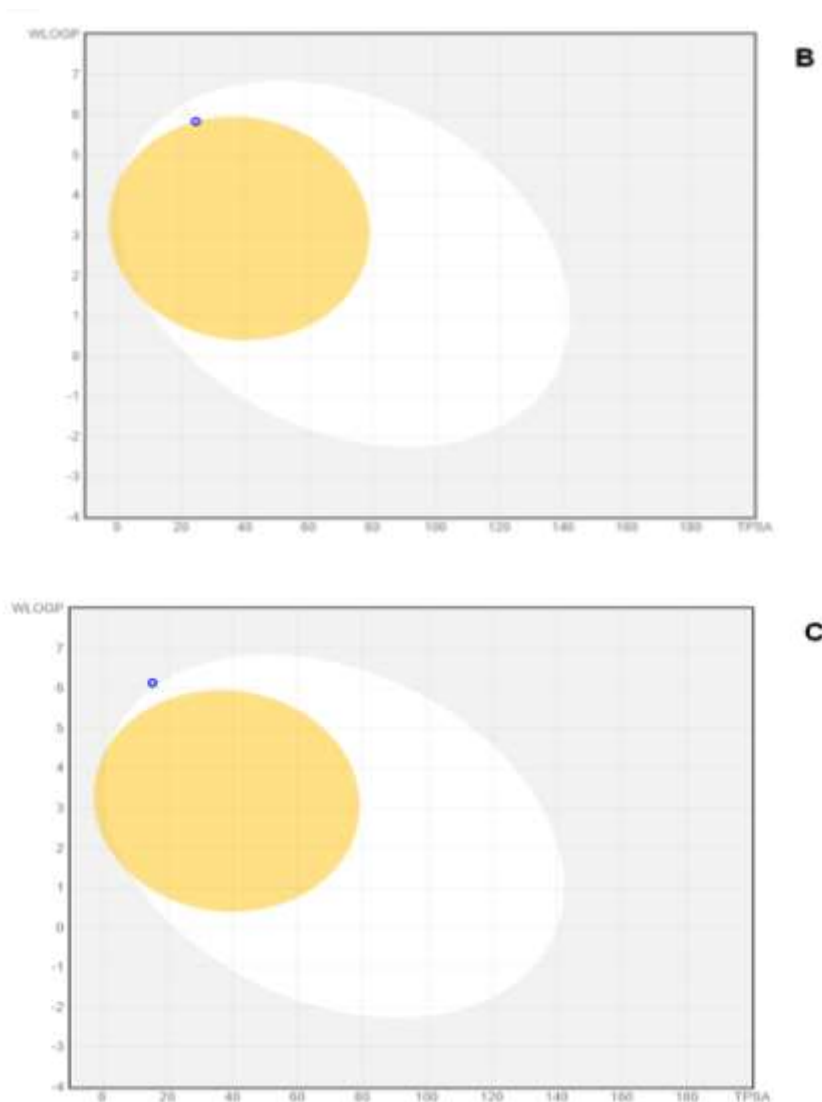
Figure 7: Boiled Egg Plot (A) Compound-2, (B) Compound-6, and (C) Compound-9.

Drug target identification

Compound-2

As the study is focused on drug repurposing, it remains crucial to determine the plausible therapeutic targets against which Compound-2 can inhibit them with micromolar concentrations, ideally. The human (*Homo sapiens*), rat (*Rattus norvegicus*), and mouse (*Mus musculus*) models revealed the inhibitory perspectives of Compound-2 against several targets like hydrolase, enzyme, oxidoreductase, Family A G protein-coupled receptor, transferase, voltage-gated ion channel, primary active transporter, ligand-gated ion channel, etc. (**Figure 8**). The predicted results strongly supported the basis of semi-synthesized natural product for possible applications against inflammation by revealing the possibilities of drug interactions with multiple targets.
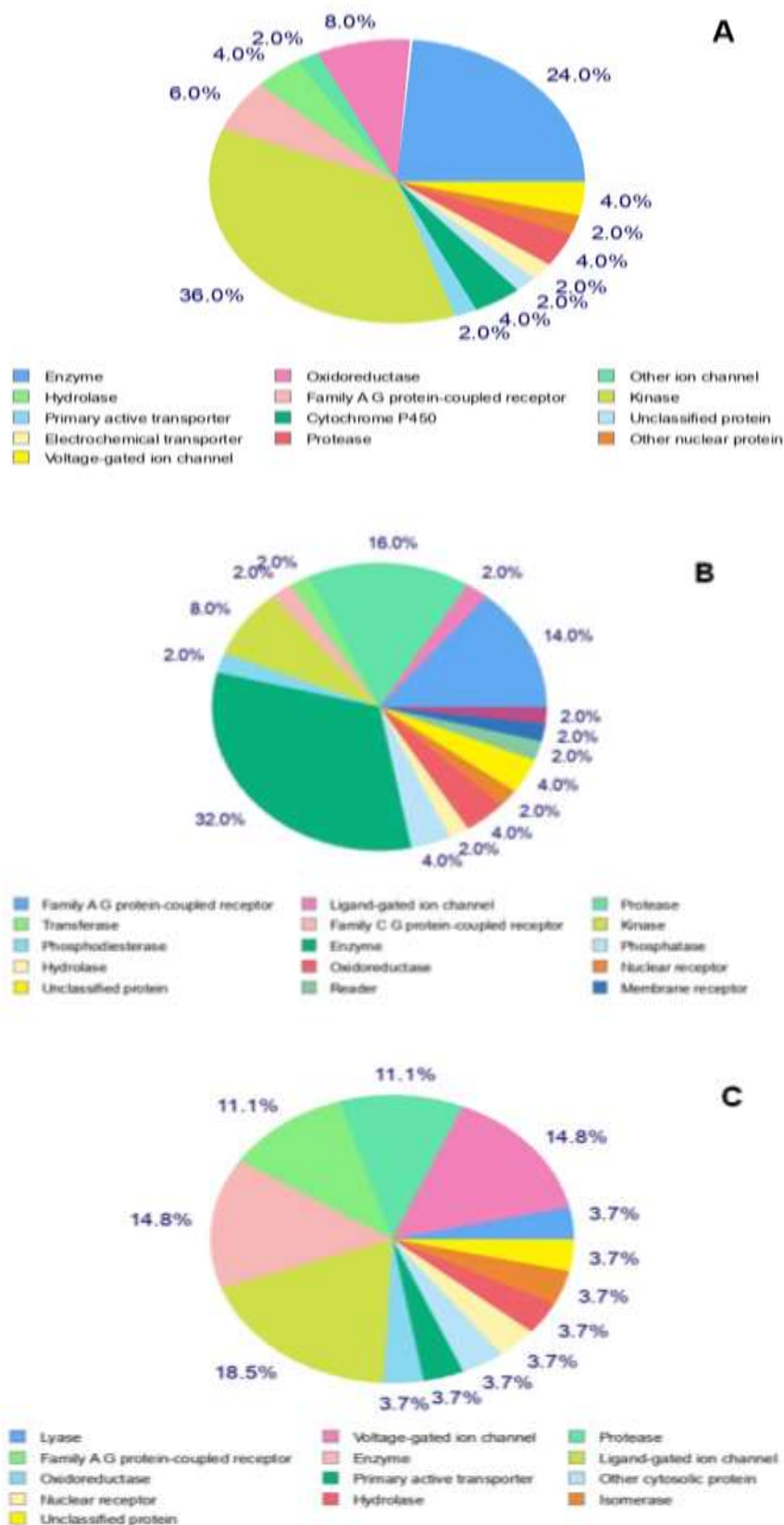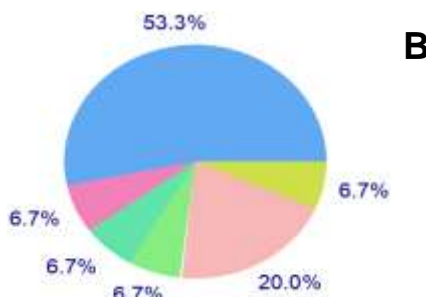
Figure 8: Predicted therapeutic targets of Compound-2 against (A) Human, (B) Mouse, and (C) Rat.

Compound-6

As the study is focused on determining the interacting profile of Compound-6 against therapeutic targets that have immense pharmacological perspectives, it remains crucial to exactly quantify the plausible therapeutic targets against which Compound-6 can inhibit them with micromolar concentrations, ideally. The human (*Homo sapiens*) model revealed the inhibitory perspectives of Compound-6 against the targets such as Family A G protein-coupled receptor (33.3%), Kinase (26.7%), Electrochemical transporter (13.3%), Protease (20%), and Hydrolase (6.7%) (**Figure 9**). The mouse (*Mus musculus*) model revealed the inhibitory perspectives of Compound-6 against the targets such as Family A G protein-coupled receptor (53.3%), Kinase (6.7%), Electrochemical transporter (6.7%), Unclassified protein (6.7%), Protease (20%), and Enzymes (6.7%). The rat (*Rattus norvegicus*) model revealed the inhibitory perspectives of Compound-6 against the targets such as Family A G protein-coupled receptor (33.3%), Ligand-gated ion channel (20%), Voltage-gated ion channel (6.7%), Electrochemical transporter (6.7%), Enzyme (6.7%), Kinase (6.7%), and Hydrolase (6.7%). The procured predicted results strongly supported the basis of interaction of this small molecule for possible applications against colorectal cancer by revealing the possibilities of interactions with multiple targets (majorly with Family A G protein-coupled receptor).

Family A G protein-coupled receptor (33.3%), Kinase (26.7%), Electrochemical transporter (13.3%), Protease (20%), Hydrolase (6.7%).

Family A G protein-coupled receptor (53.3%), **Kinase** (6.7%), **Electrochemical transporter** (6.7%), **Unclassified protein** (6.7%), **Protease** (20%), **Enzymes** (6.7%)

Family A G protein-coupled receptor (33.3%), **Ligand-gated ion channel** (20%), **Voltage-gated ion channel** (6.7%), **Electrochemical transporter** (6.7%), **Enzyme** (6.7%), **Kinase** (6.7%), **Hydrolase** (6.7%)

Figure 9: Predicted therapeutic targets of Compound-6 against (A) Human, (B) Mouse, and (C) Rat.

Compound-9

As the study is focused on determining the interacting profile of Compound-9 against therapeutic targets that have immense pharmacological perspectives, it remains crucial to exactly quantify the plausible therapeutic targets against which Compound-9 can inhibit them with micromolar concentrations, ideally. The human (*Homo sapiens*) model revealed the inhibitory perspectives of Compound-9 against the targets such as Family A G protein-coupled receptor (40%), secreted proteins (20%), other cytosolic protein (20%), enzymes (13.3%), and kinase (6.7%). The mouse (*Mus musculus*) model revealed the inhibitory perspectives of Compound-9 against the targets such as Family A G protein-coupled receptor (40%), kinase (6.7%), enzymes (6.7%), nuclear receptor (6.7%), transcription factor (6.7%), unclassified protein (6.7%), electrochemical transporter (6.7%), and other cytosolic protein (6.7%). The rat (*Rattus norvegicus*) model revealed the inhibitory perspectives of Compound-9 against the targets such as Family A G protein-coupled receptor (40%), enzymes (13.3%), voltage-gated ion channel (6.7%), ligand-gated ion channel (6.7%), kinase (6.7%), nuclear receptor (6.7%), and unclassified protein (6.7%) (**Figure 10**). The procured predicted results strongly supported the basis of interaction of this small molecule for possible applications against inflammatory targets by revealing the possibilities of interactions with multiple targets (majorly with Family A G protein-coupled receptor).
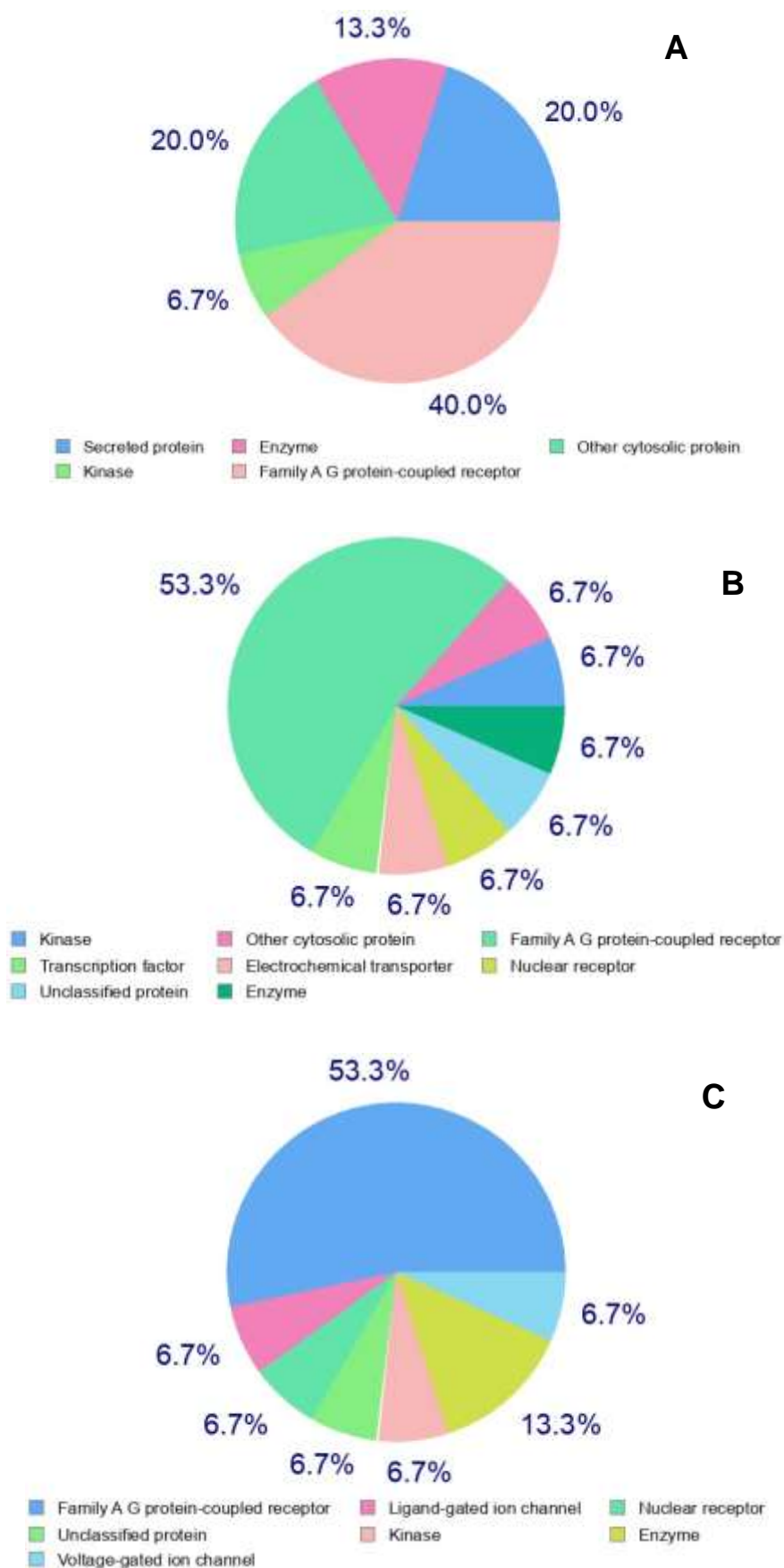
Figure 10: Predicted therapeutic targets of Compound-9 against (A) Human, (B) Mouse, and (C) Rat.

Degradation pathways for molecules

A pathway tree analysis predicts the sequential biochemical reactions that Pyrimidine might undergo, leading to its breakdown into simpler molecules. This approach combines known enzymatic reactions and metabolic pathways commonly involved in the degradation of similar compounds. The degradation of Pyrimidine is likely initiated by hydroxylation, a common metabolic transformation that introduces hydroxyl groups into the molecule. Cytochrome P_{450} enzymes, which are abundant in the liver, typically mediate this reaction. The initial hydroxylation could occur at the aromatic ring, resulting in the formation of a hydroxylated intermediate (**Figure 11**).

Following hydroxylation, the molecule may undergo further hydroxylation to form a catechol structure (adjacent dihydroxyl groups on the aromatic ring). This step enhances the molecule's solubility and prepares it for further metabolic processing. The catechol intermediate can undergo *O*-methylation, where one or both hydroxyl groups are methylated by catechol-*O*-methyltransferase (COMT). This step converts the dihydroxyl groups into methoxy groups, forming methoxy derivatives. The methoxy derivatives or the remaining hydroxyl groups can further undergo conjugation reactions such as glucuronidation or sulfation. These reactions enhance the solubility and facilitate the excretion of the compound from the body (**Figure 12**).

Enzymatic cleavage of the aromatic rings can occur, leading to the breakdown of the structure into smaller, more manageable fragments. This step is typically mediated by dioxygenases that cleave the aromatic ring between hydroxylated carbons, resulting in ring-opened products. The side chains of Pyrimidine can undergo beta-oxidation, a process commonly associated with fatty acid degradation. This step reduces the length of the aliphatic chains, producing acetyl-CoA and shorter carboxylic acids. The final breakdown products of Pyrimidine are typically small organic acids, alcohols, and CO_2, which are easily excreted from the body. The conjugated metabolites, such as glucuronides and sulfates, are excreted via urine or bile (**Figure 13**).
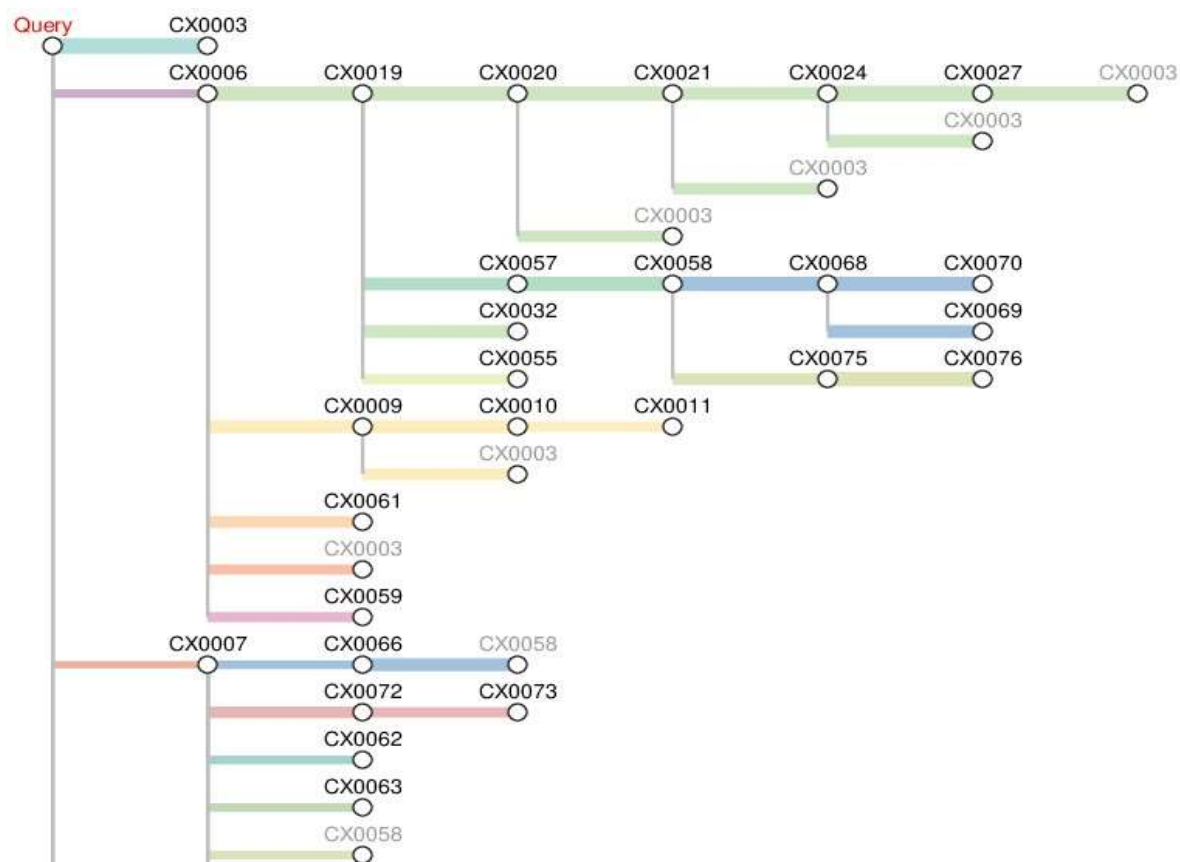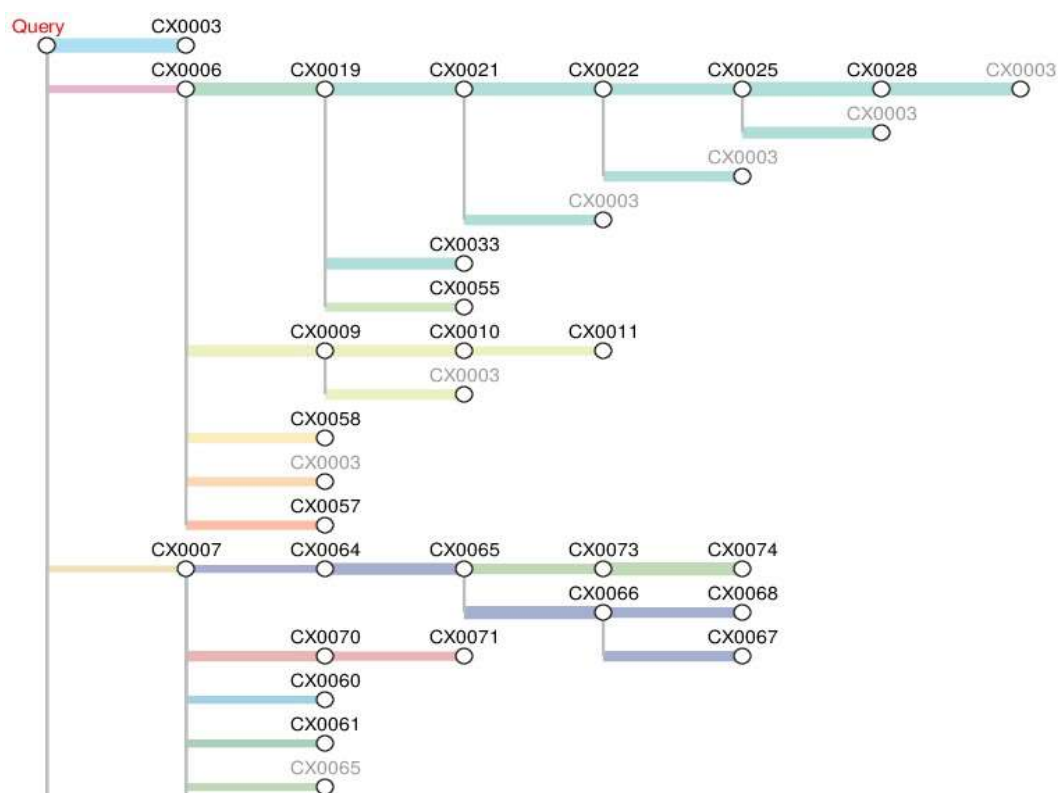
Compound-2

Figure 11: Predicted Pathway Tree for Compound-2.

Compound-6

Figure 12: Predicted Pathway Tree for Compound-6.

Compound-9

Figure 13: Predicted Pathway Tree for Compound-9.

CONCLUSION

The *in silico* research conducted on novel pyrimidine molecules has provided significant insights into their structural, electronic, and pharmacological properties. This thesis aimed to explore the potential of these molecules as candidates for therapeutic development by leveraging computational techniques to predict their behavior, stability, and interactions at the molecular level. The study began with the design and structural optimization of various pyrimidine derivatives using advanced quantum chemical methods. The geometry optimization and subsequent frequency analysis confirmed the stability of the proposed structures, with no imaginary frequencies indicating that the molecules reside at true minima on the potential energy surface. The analysis of molecular orbitals, particularly the HOMO and LUMO, provided valuable information on the electronic properties and reactivity of these compounds, highlighting key sites for electrophilic and nucleophilic attacks. Molecular docking studies were performed to assess the binding affinity of these pyrimidine derivatives with specific biological targets, which are known to play crucial roles in various diseases. The docking results revealed promising interactions, with several derivatives showing high binding affinity and favorable docking scores, suggesting their potential as lead compounds

in drug discovery. These interactions were further validated through molecular dynamics simulations, which confirmed the stability of the drug-target complexes under physiological conditions.

In addition to docking studies, the pharmacokinetic and toxicity profiles of the pyrimidine derivatives were evaluated using *in silico* ADMET (Absorption, Distribution, Metabolism, Excretion, and Toxicity) models. The results indicated that many of the novel compounds possess desirable drug-like properties, including good oral bioavailability, minimal toxicity, and favorable metabolic stability, making them strong candidates for further development. The exploration of degradation pathways through *in silico* methods provided insights into the stability and potential metabolic fate of the pyrimidine derivatives. Understanding these pathways is crucial for predicting the compounds' behavior in biological systems and for designing molecules with improved stability and efficacy. Overall, this research has demonstrated the power and effectiveness of *in silico* methods in the early stages of drug discovery. The findings from this study contribute to the growing body of knowledge on pyrimidine derivatives and their potential as therapeutic agents. While the *in silico* results are promising, it is important to note that experimental validation through *in vitro* and *in vivo* studies is necessary to confirm the predicted properties and to further develop these compounds into viable drugs. In conclusion, the novel pyrimidine molecules investigated in this thesis show considerable promise as candidates for therapeutic development. The insights gained from this in silico research lay a solid foundation for future experimental studies and pave the way for the potential application of these compounds in the treatment of various diseases. The methodologies employed in this research can also be applied to other molecular classes, underscoring the versatility and importance of computational approaches in modern drug discovery.

Conflict of interest

None declared.

REFERENCES

1. Li J, Fu A, Zhang L. An overview of scoring functions used for protein–ligand interactions in molecular docking. Interdiscip Sci Comput Life Sci., 2019; 11(2): 320–30.

2. Friesner RA, Murphy RB, Repasky MP, Frye LL, Greenwood JR, Halgren TA, et al. Extra precision Glide: Docking and scoring incorporating a model of hydrophobic enclosure for protein-ligand complexes. J Med Chem., 2006; 49(21): 6177–96.

3. Meng XY, Zhang HX, Mezei M, Cui M. Molecular Docking: A powerful approach for structure-based drug discovery. Curr Comput Aided Drug Des., 2011; 7(2): 146–57.

4. Sliwoski G, Kothiwale S, Meiler J, Lowe EW. Computational methods in drug discovery. Pharmacol Rev., 2014; 66(1): 334–95.

5. Jain AN. Surflex-Dock 2.1: Robust performance from ligand energetic modeling, ring flexibility, and knowledge-based search. J Comput Aided Mol Des., 2007; 21(5): 281–306.

6. Kitchen DB, Decornez H, Furr JR, Bajorath J. Docking and scoring in virtual screening for drug discovery: Methods and applications. Nat Rev Drug Discov, 2004; 3(11): 935–49.

7. Salmaso V, Moro S. Bridging molecular docking to molecular dynamics in exploring ligand-protein recognition process: An overview. Front Pharmacol, 2018; 9: 923.

8. Trott O, Olson AJ. AutoDock Vina: Improving the speed and accuracy of docking with a new scoring function, efficient optimization, and multithreading. J Comput Chem., 2010; 31(2): 455–61.

9. Huey R, Morris GM, Olson AJ, Goodsell DS. A semiempirical free energy force field with charge-based desolvation. J Comput Chem., 2007; 28(6): 1145–52.

10. Liu J, Wang R. Classification of current scoring functions. J Chem Inf Model, 2015; 55(3): 475–82.

11. Ferreira LG, Dos Santos RN, Oliva G, Andricopulo AD. Molecular docking and structure-based drug design strategies. Molecules, 2015; 20(7): 13384–421.

12. Lavecchia A, Di Giovanni C. Virtual screening strategies in drug discovery: A critical review. Curr Med Chem., 2013; 20(23): 2839–60.